AN AXIAL TENSILE TEST OF COMPOSITE STIFFENED PANELS WITH TWO MAN-HOLES AFTER IMPACT

Peng Shi, Qun Zhao, Jianzhuo Sun and Chuanjun Liu

Beijing Key Laboratory of Civil Aircraft Structures and Composite Materials, Beijing Aeronautical Science & Technology Research Institute of COMAC, Future Science and Technology Park, 102211, shipeng@comac.cc

Keywords: Impact, Composite, Man-hole, Stiffened panel, Axial tensile test

ABSTRACT

Three composite stiffened panels, each with two man-holes, subjected to an axial tensile load, were tested after impact. The impacts were respectively introduced on the edge of stiffener web and on the skin near a man-hole transversely. The locations, dimensions, and extensions of the damages were inspected by the ultrasonic scan system. After that, the tensile load was applied and the effects of impact damage on the panel, especially on the strain distribution, were investigated and discussed.

1 INTRODUCTION

Due to high specific strength and stiffness, composites are being used increasingly in the aerospace industry. The use of composites has brought about greater fuel efficiency and fatigue and corrosion resistance of aircraft structures. It has been applied more and more in modern aircraft designs, such as panel, rudder and fuselage. For many practical concerns, open holes, such as man-holes, are required to be designed on the aircraft lower panel. It is well known that open holes can introduce stress concentration, which leads to initiate damage and early failures. In the literature, a great number of experimental works have been done to study the mechanical behaviour of composite panels with holes, subjected to compressive[1, 2], shearing[3] and tensile[4-6] loads. Pierron et. al[7] investigated the damage process of glass-epoxy quasi-isotropic laminated by open-hole tensile test. The effect of the scaling of ply thickness was also studied. Wisnom and Hallett[8] presented several different series of open hole tension tests on quasi-isotropic IM7/8552 carbon fibre/epoxy laminates with the same stacking sequence but different ply block thicknesses and numbers of sub-laminates. Zitoune et. al[9] conducted several mechanical tests on specimens with quasi-isotropic stacking sequence with drilled holes and moulded holes. The test results revealed that, the damage mechanisms were different between the plates with drilled holes and those with moulded holes.

Impact damages often occur during the designed service life of a composite aircraft. In fact, susceptibility to low velocity impact damage is believed to be one of the main factors that limit a more widespread use of composites, although the development of toughened composites have somewhat mitigated its effect. Low velocity impact can be more of a concern as compared to high velocity impact, as it gives rise to Barely Visible Impact Damage (BVID), which might reduce the residual strength significantly without giving any visible signs of damage at the surface of structure[10]. Attention of engineers has been thoroughly aroused on composite damage tolerance design, that lead to a fact that research on the residual strength of composite panel bloomed in the last thirty years, especially experimental validation. Greenhalgh et. al[11] worked on the impact performance of structures made from carbon-fibre composites, in which the effects of structural geometry, material type and impact location were studied in skin-stringer panels representative of aircraft structure. Effects were investigated for low-velocity impacts to the skin in the bay between stringers, over a stringer foot, and over a stringer centreline. In their research, the impact damages at these locations were inspected using the ultrasonic techniques. Maalej et. al[12] investigated the characteristics of engineered cementitious composites subjected to dynamic tensile loading and high-velocity projectile impact. The performance of specimens(in penetration depth, crater size, cracking, spalling, scabbing, and fragmentation) under high-velocity hard-projectile impact was evaluated. Garnier et. al[13] compared the mechanical behavior of different impact-damaged composite materials. Three composite

materials were realized using the Liquid Resin Infusion process (LRI) according to three different cycles of polymerization. The best cycle of polymerization was determined and fatigue tests after impact were carried out to estimate the evolution of the defect.

Recently, Ostré et. al[14] presented an experimental analysis of CAEI on carbon fibre reinforced plastic (CFRP) laminates in order to determine the residual properties of the structure and to elaborate the failure scenario. The result showed that a propagation of compressive fibre failure played a major role in the mechanisms that drove the laminate residual strength after edge impact. Feng et. al[15] conducted an experimental investigation on impact damage evolution under fatigue load and shear-after-impact-fatigue (SAIF) behaviors of stiffened composite panels. Experiments were carried out with a comparison of shear on virgin specimens. Buckling/failure modes of virgin, impact and impact-fatigue specimens were obtained. Li and Chen[16] investigated the effect of low velocity edge impact damage on the damage tolerance of wing relevant composite panels stiffened with both T-shaped and I-shaped stiffeners under uniaxial compression load. Six stiffened composite panel configurations, including four specimens for each configuration, were manufactured and tested. The experimental results revealed the compression failure mechanism that local buckling, subsequent damage propagation and final fracture of the edge impacted stiffener were triggers of the final failure of a stiffened composite panel, which as well determine the ultimate load carrying capacity.

To the authors' best knowledge, in the previous work, although a great amount of experiments were conducted on the tensile, shearing and compressive characteristics of composites after impact, most of them were not in the component class but in the coupon or element level. Furthermore, tensile test on the composite stiffened panel with large man-holes after impact, is rare in the literature. In this study, a set of composite stiffened panels with two man-holes, subjected to an axial tensile load, was tested after impact. The impacts were introduced on the edge of stiffener web and on the skin near a man-hole transversely, and the damages were inspected by the ultrasonic scan system. After that, the tensile load was applied and the effects of impact damage on the panel, especially on the strain distribution, were investigated and discussed.

2 EXPERIMENTAL

2.1 Specimens

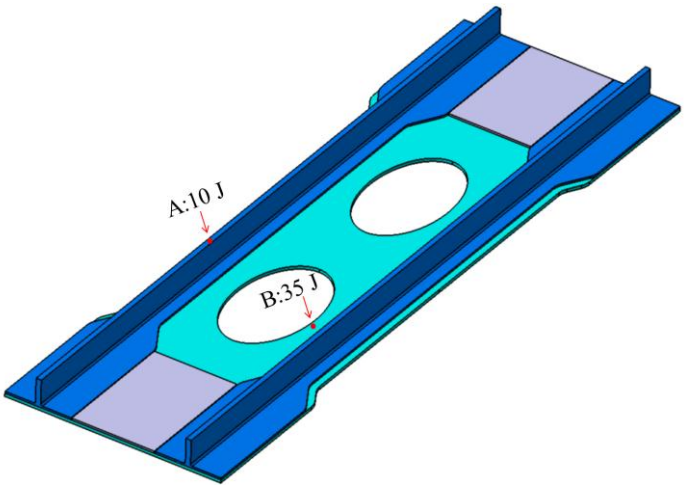

Figure 1: Specimen configuration and impact positions.

In this test, three same specimens were included, which were specified as TL01, TL02 and TL03, respectively. The specimen was a flat composite skin stiffened by two stiffeners with T-shaped cross section along the longitudinal direction. Each panel had two large elliptical man-holes and both of that had the same dimensions and areas, as can be seen in Fig.1. The specimen length was 2000mm and width was 640mm, respectively. The skin was 9 mm thick and the stringers were 440 mm apart from each other.

The material of the specimens was carbon/epoxy resin composite laminates, which was made of graphite fibre reinforced epoxy composite CYCOM X850-35-12KIM+-190. The material properties can be found in Ref.[16].

All the specimens were detected before test, by the ultrasonic scan system in order to inspect the initial defects and imperfections in the manufacturing process. The results indicated that no initial delamination or debonding interface can be found before test.

2.2 Test jigs

A pair of jigs made of steel was designed particularly to guarantee the load can be applied at the centre of the specimen cross-section to eliminate the effect of the out of plane moment. Also, the specimen was transversely supported at three lines to constrain the out of plane deformations, as can be seen in Fig.2.

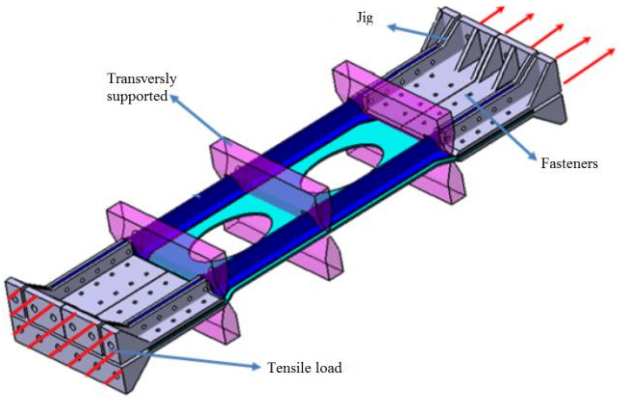

Figure 2: Jigs and out of plane support of the specimen.

2.3 Impact damages

Two impacts, one impacting on the stiffener web and the other one impacting near a hole (with a distance of 16mm from the hole edge), as can be seen in Fig.1, were introduced respectively before loading. The impact was carried out using a drop-weight tower, with a 16 mm diameter hemispherical impactor, as suggested in ASTM D7136. The impact device can be seen in Fig.3. The impact energies were specified as 10 J and 35 J for the web edge impact and the near-hole impact, respectively. The specimens were placed over three transversal supports as aircraft ribs and were restrained during the impact by means of those positions clamped, as can be seen in Fig.3.

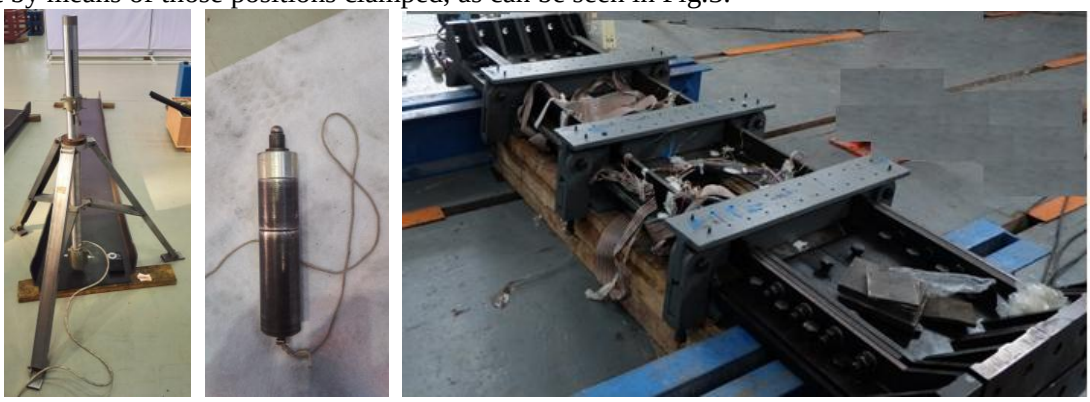

Figure 3: Impact devices and boundary conditions of the specimen.

2.4 Strain gauges

The strains were monitored by strain gauges at different positions and directions. The general configuration of the strain gauges is shown in Fig.4. Each elliptical hole was instrumented by means of

2 uniaxial strain gauges and 6 rosette strain gauges, which were bonded back-to-back on both side of the skin, to distinguish between the membrane strains and the bending strains. Also, 8 uniaxial strain gauges were bounded at each stiffener flanges and 6 uniaxial strain gauges were instrumented at each stiffener web (as can be seen in Fig.5) to monitor the strain variation with respect to the position.

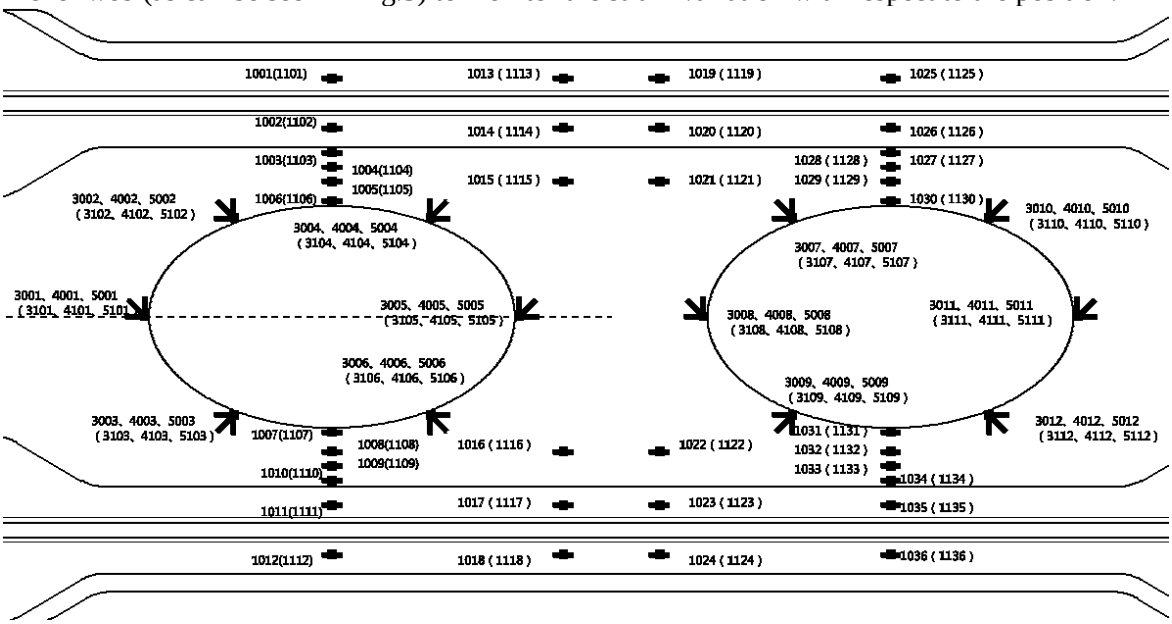

Figure 4: Strain gauges instrumented on the skin and flanges.

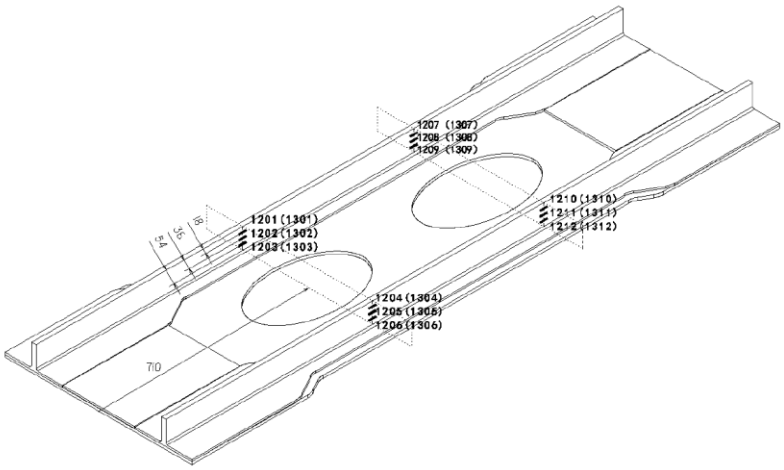

Figure 5: Strain gauges instrumented on the stiffener webs.

2.5 Test procedure

The test procedure was articulated in four main phases:

1) Impact damages were introduced. The impact energies and the dent depths were recorded, and the damage areas were inspected by using a portable ultrasonic scan device.

2) The axial tensile load was incremented in a 5% Designed Limited Load (DLL) step, up to 60% of the DLL. Meanwhile, strain levels were monitored by means of back-to-back strain gauges at each load increment, and the symmetries of strains were checked to guarantee that the difference of the back-to-back strain levels was less than 5%. Then the external load was removed. This step will be repeated for 3 times.

3) The axial load was incremented from 0 up to the 110% DLL with a step of 5% DLL. The 110% DLL will be hold for 30 seconds. Then load was decreased to 0 and the non-destructive inspection was conducted in order to observe the potential damage extension.

4) The 165% DLL was reached after the 110% DLL test with a step of 5% DLL. This load will be retained for 3 seconds. Then the load dropped to 0, and also, the non-destructive inspection was conducted in order to observe the structure had no failure.

3 EXPERIMENTAL RESULTS

3.1 Damage morphology of impact locations

Each representative impact location of all the specimens was inspected after the impact test. The edge impact of location A at the through-thickness centre of the T-shaped stiffener web was carried out firstly. The impact dents could be barely detected by visual inspection. Also, no crack can be observed on the surfaces of web edges. A portable depth measurement device was used to detect the dent depths, which were 0.16mm, 0.15mm and 0.16mm for specimens TL01, TL02 and TL03, respectively. The ultrasonic B-scan inspections were performed to identify the projection of the delamination areas over the web thickness. It showed that the full delamination area had a clear semielliptical shape, which had a major axis directed along with the longitudinal orientation of the T-shaped stiffener, and a minor axis directed along with the height of the web. Impact damage was consistent in the area for all specimens. The delamination size recorded had approximately the average major axis of 40 mm, 30 mm and 40 mm, and the average minor axis of 14 mm, 13 mm and 16 mm for specimens TL01, TL02 and TL03 respectively. An inspection also presented that existence of internal delamination was not symmetrically distributed about the mid-plane of the web.

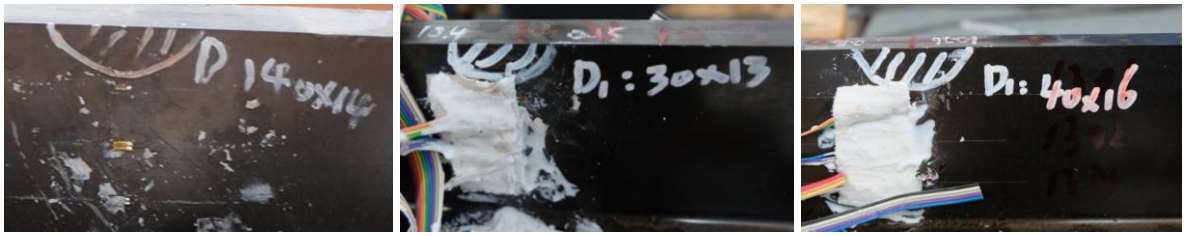

a) TL01 b) TL02 c) TL03

Figure 6: Web delamination areas of the specimens.

Specimen	Impact location A		
	Energy	Dent depth	Delamination area
TL01	10.40 J	0.16 mm	439 mm^2
TL02	10.26 J	0.15 mm	353 mm^2
TL03	10.20 J	0.16 mm	502 mm^2

Table 1: Impact damages of location A.

The transverse impact on the skin near the elliptical hole of location B was then performed. The impact dent was hardly to be observed by visual inspection. The dent depths were 0.08mm, 0.15mm and 0.06mm after measured for specimens TL01, TL02 and TL03, respectively. The C-scan and A-scan were combinedly employed to inspect the delamination near the impact locations of a radius 50mm on the skin. No skin delamination through the thickness can be detected. However, debondings were discovered at the bonding surface between the stiffener and skin in all specimens, as can be seen in Fig.7. The debonding areas are given in Table 2. Generally, this result may conclude that the geometry, boundary conditions, stiffness of the structure and transverse strength of the bonding surface could significantly affect the generation of impact damage. The near hole impact cannot lead to an obvious dent on the skin because its location was close to the hole which had a free edge, that was possibly easy for the energy dissipation. Meanwhile, when the skin was stiff enough and the boundary condition was clamped near the hole, the impact would result in the interface debonding between the stiffener and skin.

a) TL01 b) TL02 c) TL03

Figure 7: Skin-stiffener debondings after the near-hole impact.

Specimen	Impact location B		
	Energy	Dent depth	Debonding area
TL01	35.34 J	0.08 mm	22085 mm^2
TL02	35.36 J	0.15 mm	15057 mm^2
TL03	35.49 J	0.05 mm	22050 mm^2

Table 2: Impact damages of location B.

3.2 60%DLL Tests

The 60% DLL test, which was repeated three times, was significant to verify three aspects: the test machine, specimen and jigs had been set up correctly, the strains of typical locations were of symmetry, and the specimens were of consistency.

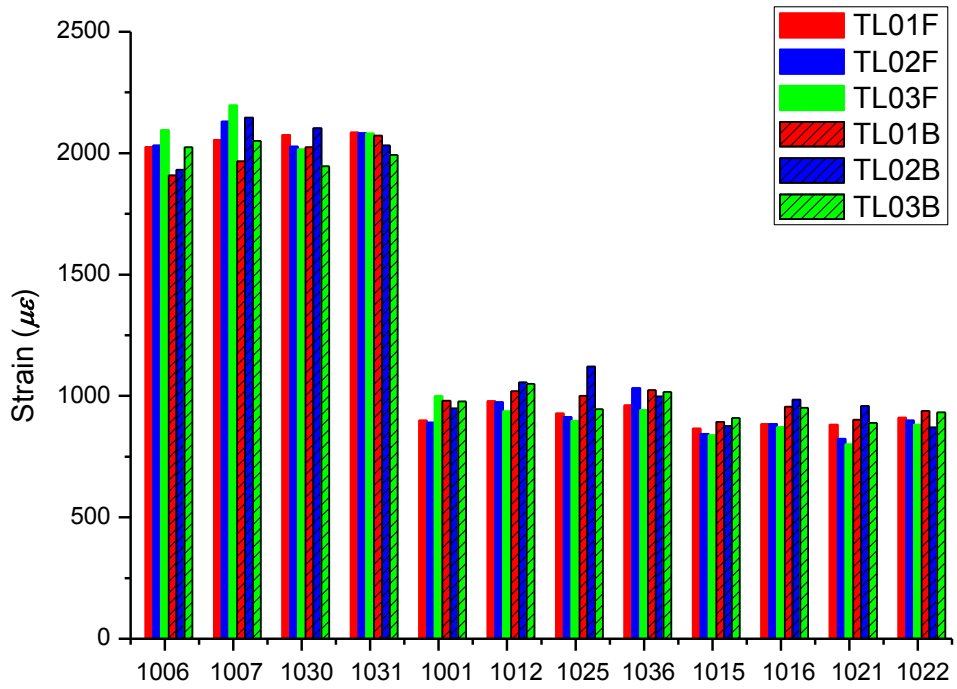

Figure 8: Strains at symmetrical locations of specimens.

The strain values at different position, including front and back gauges, with respect to different specimens were given in Fig.8. In Fig.8, strain gauge locations were manifested at the horizontal axis,

and the strain values were identified at the vertical axis. In the legend, F and B meant front gauge and back gauge, respectively.

Firstly, the strain values of the same gauge with respect to each specimen TL01, TL02 and TL03 were compared, as can be seen in Fig.8. It can be seen that the strains at the same position of the specimen TL01, TL02 and TL03 were very close. Secondly, except for the gauges bonded on the stiffener flange, the differences of back-to-back strains at the else positions were less than 5%. Thirdly, the strains at symmetrical locations on the panel, such as gauge 1006 and 1007, 1030 and 1031, etc., were much close. Most differences were less than 5%.

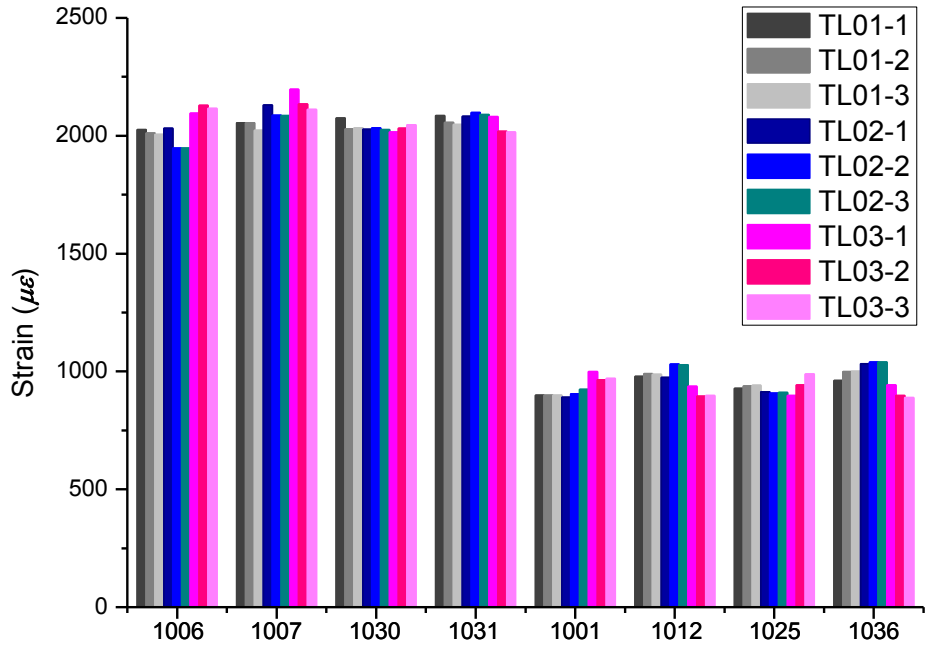

Dispersion coefficient	1006	1007	1030	1031	1001	1012	1025	1036
TL01	0.52%	0.90%	1.26%	0.94%	0.00%	0.59%	0.73%	2.19%
TL02	2.45%	1.22%	0.19%	0.39%	1.82%	3.11%	0.28%	0.45%
TL03	0.81%	2.05%	0.74%	1.82%	1.88%	2.64%	4.82%	3.14%

Figure 9: Strains at different repeated tests for each specimen.

The 60% DLL test for each specimen was repeated for three times. The dispersion coefficients were calculated to certify the consistency. As can be seen in Fig.9, strains at eight positions were illustrated, with respect to different specimens. All dispersion coefficients were less than 5%.

No sharp noise can be heard during the tests.

3.3 110% DLL and 165% DLL Tests

The 110% DLL test was carried out then. The axial load was incremented from 0 up to 110% DLL with a step of 5% DLL. When the 110% DLL reached, the tensile load was hold for 30 seconds. No piercing sound can be heard. Then the load was decreased to 0 and the non-destructive inspection was conducted. The scan results showed that no new damage occurred and no existing damage extended.

Meanwhile, a finite element analysis was performed by the commercial software Nastran. In the FEM model, the impact damages were not considered. The problem was solved based on the linearly elastic hypothesis and static formulation. The test results were compared to the FEM results, which can be seen in Table 3. Fourteen strain values of each specimen were listed. The relevant errors were calculated and the results showed that all error were less than 10%. It can be seen that generally, the FEM results were much greater than the test results.

Strain gauges	FEM results ($\mu\varepsilon$)	TL01		TL02		TL03	
		Test results($\mu\varepsilon$)	Error	Test results($\mu\varepsilon$)	Error	Test results($\mu\varepsilon$)	Error
1006	3928	3680	6.3%	3575	9.0%	3837	2.3%
1007	3929	3634	7.5%	3750	4.6%	3852	2.0%
1030	3929	3689	6.1%	3730	5.1%	3725	5.2%
1031	3929	3731	5.0%	3800	3.3%	3718	5.4%
1001	1823	1661	8.9%	1720	5.7%	1738	4.7%
1012	1823	1771	2.9%	1806	0.9%	1641	10.0%
1025	1823	1676	8.1%	1658	9.1%	1725	5.4%
1036	1823	1776	2.6%	1824	-0.1%	1648	9.6%
1004	2691	2593	3.6%	2502	7.0%	2729	-1.4%
1104	2583	2443	5.4%	2583	0.0%	2576	0.3%
1009	2691	2622	2.6%	2596	3.5%	2647	1.6%
1109	2583	2497	3.3%	2664	-3.1%	2530	2.1%
1015	1644	1558	5.2%	1534	6.7%	1562	5.0%
1115	1697	1587	6.5%	1594	6.1%	1708	-0.6%

Table 3: Comparison of the FEM and test results.

The 165% DLL was loaded next, which was reached by 5% DLL gradually. This load was retained for 3 seconds and then unloaded. No harsh noise can be heard. No damage extended, and no structural failure occurred.

It is of interest that how the debonding caused by the impact affect the near hole strain variation during the 165% DLL tension. The strains of gauge 1006, 1007, 1030 and 1031, with respect to specimens TL01, TL02 and TL03, are shown in Fig.10. It can be seen that strains of three specimens had good consistency, symmetry and agreement. During this load level, strains increased linearly and monotonously. Also, from the comparison one can see that the large debonding did not have much influence on the near-hole strains.

It is also significant to investigate the damage effect on the skin strains, especially near the damage area. Three comparisons were given, as can be seen in Fig.11, to study the difference of strains which may be caused by the skin-stiffener debonding. Four strain gauges, which were 1101, 1102, 1111 and 1112, were picked out. Comparing the strain levels of 1101 and 1112, one can see that strain value 1112 was much higher than that of 1101. Similar phenomenon can be observed between strain gauges 1102 and 1111. Furthermore, all of the specimens had this characteristic. It could be resulted from the debonding of stiffener and skin, which may decrease the stiffness of the specimen at this debonded section and lead to load re-distribution.

It is also necessary to study the effect of impact on the strain distribution directed along with the web height. Strains at four different sections, each including three strain gauges, were given in Fig.12. It should be noticed that the impact damage area was monitored by the strain gauges 1201, 1202 and 1203. From Fig.12 one can see that except for the strains of the impact area, all strains distributed almost linearly and increasingly along the direction of web height. Due to the delamination caused by the impact, strains at this area of each specimen, showed irregularly. This irregularity may be resulted from various delaminated plies and their complex interactions through the thickness of the web.

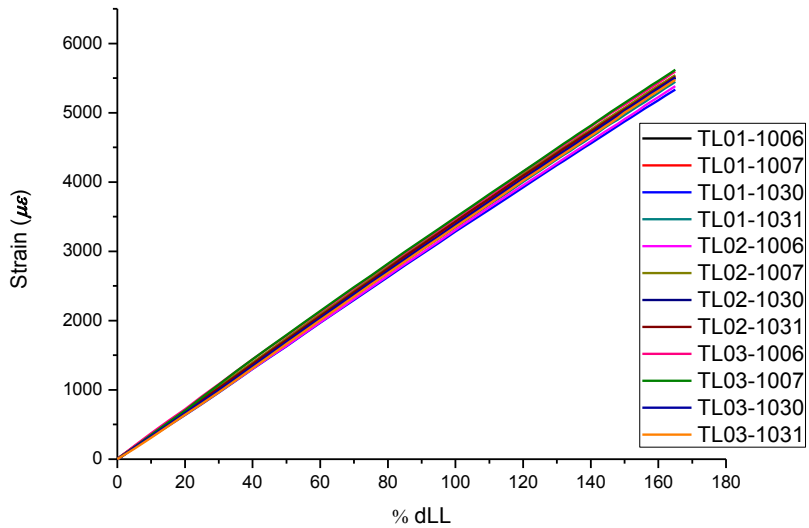

Figure 10: Near-hole strain comparison for specimens.

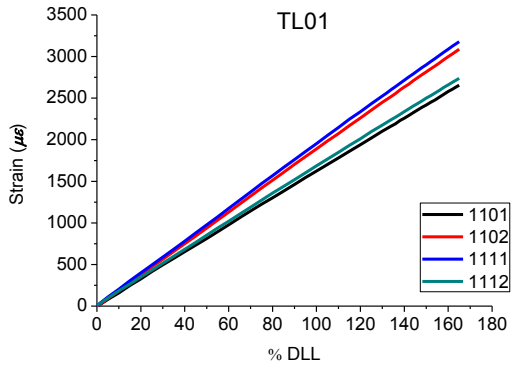

a) TL01

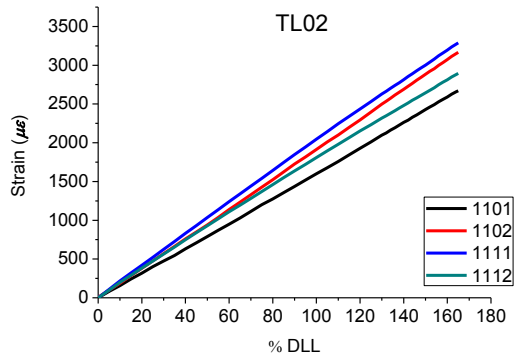

b) TL02

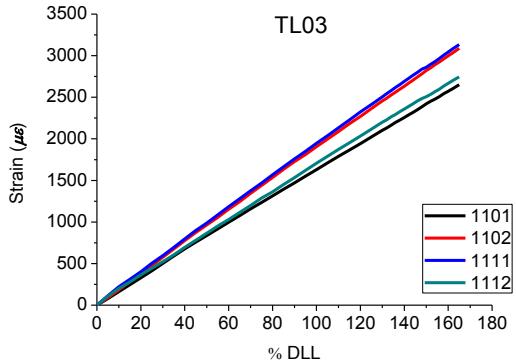

c) TL03

Figure 11: Skin strain comparison of each specimen.

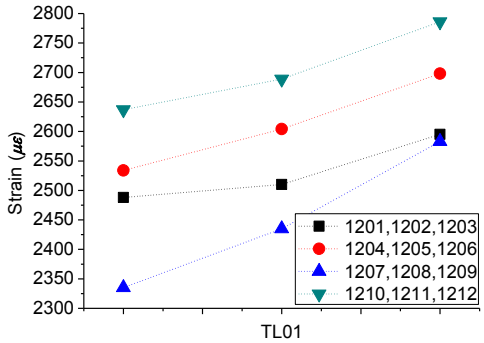

a) TL01

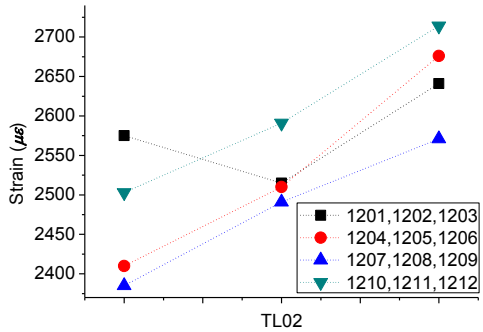

b) TL02

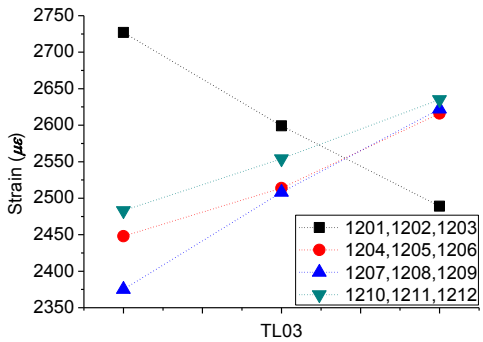

c) TL03

Figure 12: Web strain distribution of each specimen.

4 CONCLUSIONS

Three composite panel specimens, each of that was stiffened with two stringers and with two man-holes, subjected to axial tensile loading, were tested after impact. The impact damage was inspected, and its influences on the strain distribution were investigated. Test results were also compared to the FEM results. The following conclusions can be drawn from the present experimental study:

1) The presence of impact damage to the stiffener edge was apparently different from that of the skin. It might be relatively harder to be detected by visual inspection. By using an ultrasonic scan device, the full projected delamination area can be obtained and the damage inside the web approximately presented a semi-elliptical shape.

2) The near-hole impact on the skin, might not be able to lead to a visible dent and detectable delamination, but result in a detachment at the bonding surface between the stiffener and skin, where could be near the impact position. This may be affected by the geometry, boundary conditions, structure rigidity and transverse strength of the bonding surface.

3) It seems that the impact damage, even the skin-stiffener debonding, cannot affect the global strain levels much, for example, the near-hole strains, but could lead to an irregular strain distribution locally, such as the skin and web strains near the damage area.

Further experimental studies, such as the compression test and the failure test, will be carried out in the future.

REFERENCES

[1] A.N. Palazotto and T.W. Tisler, Experimental collapse determination of cylindrical composite panels with large cutouts under axial load, *Composite Structures*, **12**, 1989, pp. 61-78.

[2] J. Eiblmeier, The buckling response of carbon fibre composite panels with reinforced cut-outs, *Composite Structures*, **32**, 1995, pp. 97-113.

[3] X. Li, W. Gao and W. Liu, The bearing behaviour and failure characteristic of CFRP laminate with cutout under shearing load: Part I. Experiments, *Composite Structures*, **141**, 2016, pp. 355-365.

[4] J. Backlund and C. Aronsson, Tensile fracture of laminates with holes, *Journal of Composite Materials*, **20**, 1986, pp. 259-286.

[5] L. Toubal, M. Karama and B. Lorrain, Stress concentration in a circular hole in composite plate, *Composite Structures*, **68**, 2005, pp. 31-36.

[6] E. Abisset, F. Daghia and P. Ladevèze, On the validation of a damage mesomodel for laminated composites by means of open-hole tensile tests on quasi-isotropic laminates, *Composite*: *Part A*, **42**, 2011, pp. 1515-1524.

[7] F. Pierron, B. Green, M.R. Wisnom and S.R. Hallett, Full-field assessment of the damage process of laminated composite open-hole tensile specimens. Part II: Experimental results, *Composite*: *Part A*, **38**, 2007, pp. 2321-2332.

[8] M.R. Wisnom and S.R. Hallett, The role of delamination in strength, failure mechanism and hole size effect in open hole tensile tests on quasi-isotropic laminates, *Composite*: *Part A*, **40**, 2009, pp. 335-342.

[9] R. Zitoune, L. Crouzeix, F. Collombet, T. Tamine and Y.H. Grunevald, Behaviour of composite plates with drilled and moulded hole under tensile load, *Composite Structures*, **93**, 2011, pp. 2384-2391.

[10] M.O.W. Richardson and M.J. Wisheart, Review of low-velocity impact properties of composite materials, *Composite*: *Part A*, **27**, 1996, pp. 1123-1131.

[11] E.S. Greenhalgh, S. Bishop, D. Bray, D. Hughes, S. Lahiff and B. Millson, Characterisation of impact damage in skin-stringer composite structures, *Composites Structures*, **36**, 1996, pp. 187-207.

[12] M. Maalej, S.T. Quek and J. Zhang, Behavior of hybrid-fiber engineered cementitious composites subjected to dynamic tensile loading and projectile impact, *Journal of Materials in Civil Engineering*, **17**, 2005, pp. 143-152.

[13] C. Garnier, M.L. Pastor, B. Lorrain and O. Pantalé, Fatigue behavior of impacted composite structures, *Composite Structures*, **100**, 2013, pp. 443-450.

[14] B. Ostré, C. Bouvet, C. Minot and J. Aboissière, Experimental analysis of CFRP laminates subjected to compression after edge impact, *Composite Structures*, **152**, 2016, pp. 767-778.

[15] Y. Feng, Y. He, X. Tan, T. An and J. Zheng, Investigation on impact damage evolution under fatigue load and shear-after-impact-fatigue (SAIF) behaviors of stiffened composite panels, *International Journal of Fatigue*, **100**, 2017, pp. 308-321.

[16] N. Li and P.H. Chen, Experimental investigation on edge impact damage and Compression-After-Impact (CAI) behavior of stiffened composite panels, *Composite Structures*, **138**, 2016, pp. 134-150.